Molecular Cell Biology

Cancer Research

LINC00261 Is an Epigenetically Regulated Tumor Suppressor Essential for Activation of the DNA Damage Response

Shandy Shahabi[1], Vishaly Kumaran[1], Jonathan Castillo[1,2,3], Zhengmin Cong[1], Gopika Nandagopal[1], Daniel J. Mullen[1,2,3], Alexander Alvarado[1], Michele Ramos Correa[3], Autumn Saizan[3], Riya Goel[3], Amrita Bhat[3], Sean K. Lynch[4], Beiyun Zhou[3,5,6], Zea Borok[1,3,5,6], and Crystal N. Marconett[1,2,3]

Abstract

Lung cancer is the leading cause of cancer-related death in the United States. Long noncoding RNAs (lncRNA) are a class of regulatory molecules whose role in lung carcinogenesis is poorly understood. In this study, we profiled lncRNA expression in lung adenocarcinoma (LUAD) cell lines, compared their expression with that of purified alveolar epithelial type II cells (the purported cell of origin for LUAD), cross-referenced these with lncRNAs altered in the primary human tumors, and interrogated for lncRNAs whose expression correlated with patient survival. We identified *LINC00261*, a lncRNA with unknown function in LUAD, adjacent to the pioneering transcription factor FOXA2. Loss of *LINC00261* was observed in multiple tumor types, including liver, breast, and gastric cancer. Reintroduction of *LINC00261* into human LUAD cell lines inhibited cell migration and slowed proliferation by inducing G_2–M cell-cycle arrest, while upregulating DNA damage pathway genes and inducing phosphorylation-mediated activation of components of the DNA damage pathway. FOXA2 was able to induce *LINC00261* expression, and the entire locus underwent hypermethylation in LUAD, leading to loss of expression. We have thus identified an epigenetically deregulated lncRNA, whose loss of expression in LUAD promotes the malignant phenotype and blocks activation of the DNA damage machinery, predisposing lung cells to cancer development.

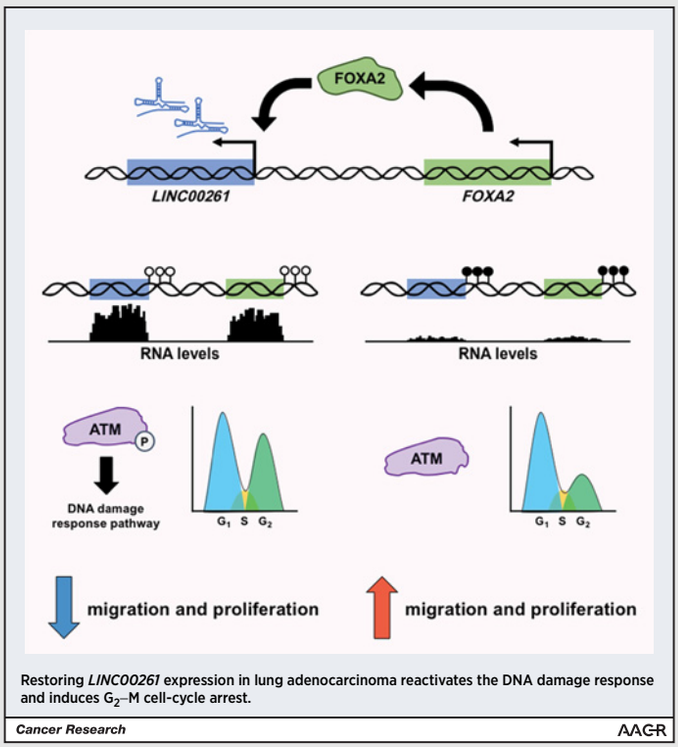

Restoring *LINC00261* expression in lung adenocarcinoma reactivates the DNA damage response and induces G_2–M cell-cycle arrest.

Cancer Research AACR

Significance: These findings identify *LINC00261* as a tumor suppressor that blocks cellular proliferation by activating the DNA damage response and suggest that epigenetic therapy to inhibit DNA methylation may enhance treatment of LUAD.

Graphical Abstract: http://cancerres.aacrjournals.org/content/canres/79/12/3050/F1.large.jpg.

See related commentary by Davalos and Esteller, p. 3028

[1]Department of Biochemistry and Molecular Medicine, Keck School of Medicine, University of Southern California, Los Angeles, California. [2]Department of Surgery, Keck School of Medicine, University of Southern California, Los Angeles, California. [3]Norris Comprehensive Cancer Center, Keck School of Medicine, University of Southern California, Los Angeles, California. [4]Department of Product Engineering, Division of Manufacturing Operations, MAXIM Integrated Products, Sunnyvale, California. [5]Division of Pulmonary, Critical Care and Sleep Medicine, Department of Medicine, Keck School of Medicine, University of Southern California, Los Angeles, California. [6]Hastings Center for Pulmonary Research, Keck School of Medicine, University of Southern California, Los Angeles, California.

Note: Supplementary data for this article are available at Cancer Research Online (http://cancerres.aacrjournals.org/).

S. Shahabi and V. Kumaran contributed equally to this article.

Corresponding Author: Crystal N. Marconett, Norris Comprehensive Cancer Center, Keck School of Medicine, University of Southern California, NTT 6418A M/C 9176, Los Angeles CA 90089-9520. Phone: 323-865-0649; Fax: 323-865-0158; E-mail: Crystal.Marconett@med.usc.edu

Cancer Res 2019;79:3050–62

doi: 10.1158/0008-5472.CAN-18-2034

Introduction

Lung cancer continues to be the leading cause of cancer-related death in the United States, with approximately 150,000 deaths reported annually (1, 2). Annual deaths attributed to lung cancer surpass colorectal, breast, and prostate cancers combined (3). Non–small cell lung cancer (NSCLC) represents the majority of new lung cancer cases, encompassing approximately 85% of all diagnosed lung cancers (4). Among NSCLC, the most commonly occurring subtype in the United States is lung adenocarcinoma (LUAD; ref. 1). Understanding the specific drivers of LUAD can aid in developing targeted therapies, which has been effective for several other cancers (5, 6). Analysis of significant driver mutations in LUAD has identified KRAS, EGFR, and EML4-ALK translocations as the most prevalent mutations, present in over half of all cases (7). Targeted therapy directed toward EGFR mutations has shown a positive response to the tyrosine kinase inhibitors, such as gefitinib and erlotinib (8). However, resistance soon arises, leading to overwhelming relapse rates (9–11). Furthermore, of LUAD cases screened, approximately 30% harbor no known oncogenic driver mutations (12, 13), emphasizing the need for a deeper understanding of the molecular mechanisms underlying carcinogenesis.

RNAs play many roles in cellular physiology, regulating processes integral to cellular survival. Long noncoding RNA (lncRNA) transcripts are a largely uncharacterized subtype of RNA defined as transcripts greater than 200 nucleotides in length with little to no protein-coding capacity. Their high tissue specificity and temporal expression patterns suggest that they serve highly significant functions throughout the development (14). In addition, lncRNAs exert a variety of functions throughout the cell, acting *in cis* locally or *in trans* at different loci throughout the genome, playing critical roles in gene regulation and the development of cancer (15–17).

Large-scale profiling studies, such as that performed by The Cancer Genome Atlas (TCGA), have revealed thousands of differentially expressed lncRNAs in multiple cancers (12, 18), yet little is known of how these candidates function at a molecular level to regulate cellular phenotypes (19). In addition, epigenetic alterations to lncRNA expression have been suggested to contribute to the cancer phenotype (20, 21). Only a few lncRNAs have been implicated in LUAD development (22–25), including *H19*, *ANRIL*, *MEG3*, *NEAT1*, and *MALAT1* (25). The mechanisms of action for these lncRNAs are diverse, underscoring both the pivotal roles lncRNAs play in the development of cancer and our current limited understanding of lncRNAs' full role in the pathogenesis of this disease.

We performed transcriptome-wide bioinformatic analysis coupled with molecular characterization of the candidates to determine the functional relevance for lncRNAs with potential therapeutic applications in LUAD. *LINC00261* was identified as being significantly downregulated in LUAD. Functional genomic studies demonstrated a fundamental role for *LINC00261* in regulating G_2–M cell-cycle checkpoint arrest through activation of ATM phosphorylation. *LINC00261* expression was lost in LUAD through epigenetic silencing of the *LINC00261-FOXA2*, a transcription factor locus, and removal of DNA methylation silencing was able to reactivate *LINC00261* expression. Our results identify *LINC00261* as a novel tumor suppressor, whose epigenetic suppression results in worsening LUAD outcomes.

Materials and Methods

Cell lines and primary cells

LUAD cell lines were obtained from the laboratory of E. Haura or the ATCC and fingerprinted to verify their identity prior to experimentation at the University of Arizona (Tucson, AZ). Cells were verified *Mycoplasma*-free every 2 months in the laboratory via established protocols (26). Remnant human transplant lungs were obtained in compliance with Institutional Review Board–approved protocols for the use of human source material in research (HS-07-00660) and processed within 3 days of death. Lungs were processed for primary alveolar epithelial type II cell isolation as in ref. 27.

RNA- and whole-genome bisulfite-sequencing and high-dimensional analysis

For the cell lines and purified alveolar epithelial cells (AEC), 1 μg of RNA underwent RiboZero (Illumina) depletion and subsequent library preparation using the Illumina TruSeq Kit (Illumina). Samples were multiplexed and underwent paired-end 50-bp sequencing on the Illumina HiSeq2000. FASTQ files were processed to remove the bases 1–12 of all the reads and low sequence complexity elements. Filtering was performed to retain only the reads with the Quality scores >20 for 90% of the read length. Once cleaned, FASTQ files were aligned to the Lincipedia2.1 transcriptome and RefSeqv58 (hg19) using Bowtie version 1.1. Transcripts were eliminated that had fewer than 10 reads across the dataset before differential analysis using EdgeR. For the transgenic H522-CMV-*LINC00261* and H522-CMV-NEO controls, 1 μg of RNA underwent library preparation as above, then single-end 76-bp sequencing using the Illumina NextSeq 500 and analysis using Edge R. Raw FASTQ files were cleaned as above and aligned to the RefSeqv77 (hg38) transcriptome. Whole-genome bisulfite sequencing (WGBS) processing and analysis were described previously (28).

PCR for cloning *LINC00261* and promoter fragments

LINC00261 was synthesized in two segments using different methods due to high CpG and low complexity in the different fragments. The Phusion High-Fidelity DNA Polymerase kit (New England Biolabs) was used for the PCR amplification of the major exon of *LINC00261*. The single-stranded DNA oligonucleotide primers (Integrated DNA Technologies, IDT) used for PCR reactions are listed in Supplementary Table S1. Human genomic DNA (Promega) was used as the template for all PCR reactions. The PCR reaction consisted of 1× Phusion HF buffer, 200 μmol/L dNTPs, 0.5 μmol/L forward primer, 0.5 μmol/L reverse primer, 150 ng template genomic DNA from a human male (G147A, Promega), 3% DMSO, 0.3 μL Phusion DNA polymerase, and water to a total volume of 30 μL. *LINC00261* upstream exons 1–3 were synthesized by IDT-DNA using their gene synthesis technology and cloned along with the major exon into the pCMV6-vector backbone (PS100001, Origene).

Generation of stable cell lines expressing *LINC00261*

Mycoplasma-negative A549 cells underwent single-nucleotide polymorphism typing for cell-line verification and were then transfected with either the linearized *LINC00261* shRNA construct or scrambled control shRNA (HC137604, Origene). A total of 7×10^4 cells per well were plated into 24-well dish and puromycin (0.625 μg/mL) was used for selection. H522 LUAD cells were

transfected with either the linearized full-length *LINC00261* plasmid or the control C-terminal Myc-DDK–tagged pCMV-6 entry vector. Optimized transfection conditions for H522 cells consisted of 8×10^4 cells per well with a G418 concentration of 166 μg/mL. Stable cell lines were assayed by qRT-PCR every third passage to verify stable knockdown was maintained.

Data access

All datasets are deposited in the public Gene Expression Omnibus database (GSE110025).

RNA isolation and qRT-PCR

RNA was harvested from cells using TRIzol reagent according to the manufacturer's protocol (Sigma). cDNA was prepared using the iScript cDNA Synthesis Kit (Bio-Rad) according to the manufacturer's protocol.

Proliferation assay

Cell proliferation was measured by seeding 1×10^4 cells per well in sets of 4 wells in a 24-well dish. One well of each set was trypsinized at 24-hour intervals over a period of 4 days and counted using a Bright-Line hemocytometer (Sigma-Aldrich). Three technical replicates were performed on three different stably transfected cell lines per assay.

Transwell migration and invasion assay

Transwell migration and invasion assays were performed as described previously (29). Briefly, cell migration was measured using Corning Transwell inserts (8-μm pore size, Corning). In each well, 5×10^4 cells were added to the top chamber and suspended in 100 μL of serum-free medium (RPMI 1640, 1% penicillin/streptomycin, 0.1% BSA; RMBIO). In the bottom chamber, 600 μL of the complete medium (RPMI 1640, 1% penicillin/streptomycin, 10% FBS) was added. After 24-hour incubation, the top of the membrane was dried with a cotton swab to remove any remaining nonmigrated cells. Transwell inserts were fixed with 70% ethanol for 10 minutes, dried, and stained with 0.2% crystal violet (Santa Cruz Biotechnology). Using an inverted microscope with a magnification of ×100, migrated cells were counted in three randomly selected fields and averaged. Cell invasion was measured by coating wells with 15 μg of Matrigel (Corning) diluted in 0.01 mol/L Tris (pH 8.0) and 0.7% NaCl (Promega; Amresco) and allowing them to dry for 4 hours at 37°C prior to adding cells. Three biological and technical replicate experiments were performed for each assay.

Soft-agar assay

Colony formation was measured by suspending 2,000 cells in soft-agar growth medium (0.3% agar, 1× RPMI1470, 1% penicillin/streptomycin, 10% FBS) in 6-well plates precoated with a solidified 0.5% agar/culture medium base. Twice a week, 100 μL of the culture medium was added to the top of the agar layer. After three weeks, cells were stained with 6.0% glutaraldehyde and 0.1% crystal violet and imaged using an Olympus IX51, an inverted system microscope (×40 magnification) with Olympus Qcolor3 camera. Quantification was performed by counting colonies from three random fields using QCapture Software in three biological replicates. A colony is defined as the area >10,000 μm^2. Three technical replicates were performed for each assay.

Flow cytometry

Cells were plated onto Corning 6-well tissue culture dishes (Corning). Once 70% confluent, cells were hypotonically lysed in 300 μL of the DNA staining solution consisting of 0.5 mg/mL propidium iodide (PI), 0.1% sodium citrate, 0.05% Triton X-100 (Sigma-Aldrich). Lysates were filtered using a 40-μm nylon cell strainer (BD Falcon) to remove cell membranes and debris. PI-stained nuclei were detected using a PL-2 detector with a 575-nm band-pass filter on a Beckman-Coulter FACS analyzer with laser output adjusted to 488 nm. A total of 1×10^4 nuclei from the total population were analyzed per sample at a rate of 100–200 nuclei/second. The percentages of cells within the G_1, S, and G_2–M phases of the cell cycle were determined by analyzing the output histogram using FlowJo v10.1. Technical triplicates were averaged and statistics performed on three biological replicates.

Scratch assay

A total of 4×10^5 cells per well were plated into a 6-well dish and the cells were grown to confluence. The plate was then vertically scratched using a P20 pipette tip, and visually inspected using an inverted phase contrast microscope. After 24 hours, the cells were washed with PBS and media were replaced, followed by visualization. The plates were then analyzed with T-Scratch software (30). The protocol was modified from ref. 31. Technical quadruplicates were averaged and statistics performed on three biological replicates.

Tumor xenografts

All mouse experiments were approved by the Institutional Animal Care and Use Committee (IACUC) of University of Southern California protocol # 20633. Eight-week-old female athymic nude mice were purchased from Jackson Laboratory (Jackson Laboratory). All animal studies were performed in compliance with the University of Southern California IACUC guidelines. H522 CMV-NEO and CMV-*LINC00261* cells were suspended in 150 μL PBS with 50% Matrigel and subcutaneously injected in the dorsal flanks of mice (1×10^6 cells per flank). Tumors were measured three times per week and their volumes (V) are calculated by the previously published formula $V = lw^2/2$, where l and w are the larger and smaller length diameters, respectively (32). Mice were euthanized after 6 weeks by intraperitoneal injection of Euthasol at the experiment endpoint and tumors were excised and weighed.

Western blot analysis

Total protein lysates were obtained from both H522-CMV-*LINC00261* cells and H522-CMV-NEO controls using radioimmunoprecipitation assay (RIPA) buffer containing 1 mmol/L phenylmethylsulfonyl fluoride. Protein lysates were run on 10% Tris polyacrylamide gels and then electrophoretically transferred to Immuno-Blot polyvinylidene difluoride membranes. The membranes were then incubated overnight at 4°C with antibodies from Cell Signaling Technology DNA Damage Repair Kit (CS#9947) as well as β-actin (Cell Signaling Technology #4970), BRCA2 (Origene #TA313520), and phospho-BRCA2 (Invitrogen #PA537499). The membranes were blocked for 1 hour in 5% nonfat dry milk at room temperature and horseradish peroxidase (HRP)-conjugated goat anti-rabbit immunoglobulin was applied at a dilution of 1:10,000 for 2 hours at room temperature. HSP90 (GTX109753, GeneTex, 1:1,000) was used as a loading control and the blots were visualized using a

Molecular Image ChemiDoc XRS+ (Bio-Rad). The analysis software used was ImageJ (NIH, Bethesda, MD). Ku-55933 (Sigma-Aldrich) was used as a specific inhibitor of ATM kinase phosphorylation. Representative blots of three independent experiments are shown.

Luciferase reporter assay

Constructs were transfected into A549 cells using FugeneHD (Promega) and H522 cells using Lipofectamine 2000 (Thermo Fisher Scientific). Luciferase assays were conducted as described previously (28). Technical triplicates were averaged and statistics performed on three biological replicates.

Statistical analysis

Statistics for biological experiments were calculated using Prism5. Two-sided paired *t* tests were used for cell line comparisons between test and controls. ANOVA was used for trend tests. *P* values are denoted as follows: *, ≤ 0.05; **, ≤ 0.01; ***, ≤ 0.001.

Results

Identification of *LINC0261* as a tumor suppressor in LUAD

To identify LUAD-specific candidate lncRNAs, we analyzed 16 different LUAD cell lines for their whole lncRNA transcriptome as defined by lincipedia2.1 (Supplementary Fig. S1A). This revealed approximately 32,000 lncRNAs expressed to some level in LUAD. Differentially expressed lncRNAs between cancerous cells and normal human alveolar epithelial cells (AEC), the purported cells of origin for LUAD, were identified by comparing LUAD cell lines to previously generated whole transcriptomic profiling of purified AECs from three human donor lungs not used for transplant (27). Comparison of lncRNA expression revealed that 833 lncRNA transcripts (649 genes) were differentially expressed between LUAD cell lines and AECs (Supplementary Fig. S1B; Supplementary Table S2). To exclude lncRNAs differentially expressed due to effects of *in vitro* cell culture, we compared this set of lncRNAs to those differentially expressed in publicly available datasets of primary human LUAD tumors profiled by TCGA, as previously determined by Mather and colleagues (33), resulting in a narrowed list of 16 lncRNAs with potential relevance in both primary human tumors and cell line model systems.

While previous transcriptomic analyses have determined that thousands of genes are differentially expressed in cancers when compared with the adjacent normal tissues, few are "drivers" of carcinogenesis. The majority of alterations are "passive" and the result of tumorigenesis, not causal. To assess which of these lncRNAs may be driving carcinogenesis, we evaluated the survival outcomes and stage at loss of expression. Six of the candidate 16 lncRNAs had significant effects on survival, and *LINC00261* emerged as the top candidate with a dramatic stage-dependent effect on expression (Fig. 1A) and survival (Fig. 1B). Using qRT-PCR, *LINC00261* was significantly downregulated in the panel of LUAD cell lines compared with the purified primary AECs (Fig. 1C). To determine whether the loss of expression was LUAD-specific or more generalized phenomenon across cancer types, we extracted the expression of *LINC00261* in many TCGA-profiled cancer types using lncRNAtor (34). *LINC00261* loss is observed in multiple epithelial cancers (Fig. 1D), with the effects on survival and stage-dependent expression in liver and breast (Supplementary Fig. S2A and S2B) as well as previous reports in gastric cancer (35), indicating that *LINC00261* is a candidate of high interest as a potential tumor suppressor across multiple epithelial cancer types. In addition, *LINC00261* expression was significantly correlated with tobacco smoking history in LUAD, suggesting an environmental trigger may initiate loss of this gene in the development of cancer (Supplementary Fig. S2C).

LINC00261 expression reduces proliferation, migration, and initiates G_2–M cell-cycle arrest in LUAD cells

To determine whether *LINC00261* plays a functional role in LUAD carcinogenesis, we constructed an ectopic expression vector containing a CMV promoter and the full-length *LINC00261* transcript. H522 LUAD cell lines were chosen for ectopic reintroduction as they lack endogenous *LINC00261* expression (Supplementary Fig. S3A). Stable reintroduction of the CMV construct resulted in a level of expression equivalent to the endogenous levels of *LINC00261* expression in the primary AECs (Supplementary Fig. S3B). Ectopic expression of *LINC00261* resulted in a significant decrease in proliferation of H522 cells (Fig. 2A, $P < 0.01$) relative to CMV-NEO vector control over the course of four days. In addition to increased proliferation, one of the hallmarks of cancer is the acquisition of migratory capacity, leading to metastasis. The migratory capability of H522 CMV-*LINC00261*–stable cell lines was tested through a scratch assay. *LINC00261* was able to decrease the migration of H522 LUAD cells compared with NEO controls (Fig. 2B). Quantification over the course of four independent experiments using TScratch revealed that *LINC00261* significantly reduces migratory capacity *in vitro* (Supplementary Fig. S3C).

To determine how *LINC00261* blocks cellular proliferation, we performed cell-cycle analysis on H522-CMV-*LINC00261* and H522-CMV-NEO controls. FACS analysis demonstrated that reintroduction of *LINC00261* arrests H522 cells in the G_2–M phase of the cell cycle (Fig. 2C; Supplementary Fig. S3D). Quantification revealed a significant shift in the population from the G_0–G_1 to the G_2–M phase of the cell cycle (Fig. 2D). Finally, a key hallmark of defining a gene as a tumor suppressor is the ability to inhibit tumor formation *in vivo*. H522-CMV-*LINC00261* cells alongside CMV-NEO controls were implanted into nude mice and the growth of tumors was measured for 6 weeks. *LINC00261* resulted in decreased tumor weight as compared with NEO-treated mice controls (Fig. 2E). *LINC00261* was also able to inhibit tumor growth over time (Fig. 2F). *LINC00261*-expressing tumors also showed a decrease in vascularization relative to the empty vector controls (Fig. 2G).

While the majority of LUAD primary tumors and LUAD cell lines lack the expression of *LINC00261*, there are few stage 4 primary tumors and aneuploid cell lines that express measurable endogenous *LINC00261*, including the A549 LUAD cell line (Fig. 1C). To determine whether the ablation of *LINC00261* was able to affect the hallmarks of cancer phenotypes, we generated stably knocked down *LINC00261* using short hairpin RNAs (A549-sh*LINC00261*) in A549 cells, one of the cell lines that expresses endogenous *LINC00261* (Fig. 3A). Ablation of *LINC00261* in A549 cells caused a significant increase in A549 cell proliferation (Fig. 3B), and also significantly increased colony formation (Fig. 3C and D) and invasion (Fig. 3E and F). Migration of A549 cells was also affected by the knockdown of *LINC00261*; however, this result did not reach statistical significance (Supplementary Fig. S4A). FACS analysis of A549-sh*LINC00261* showed a significant increase in the proportion of cells with >G2 DNA content (Fig. 3G and H), suggesting that the lack of *LINC00261* results in chromosomal instability and aneuploidy. Consistent

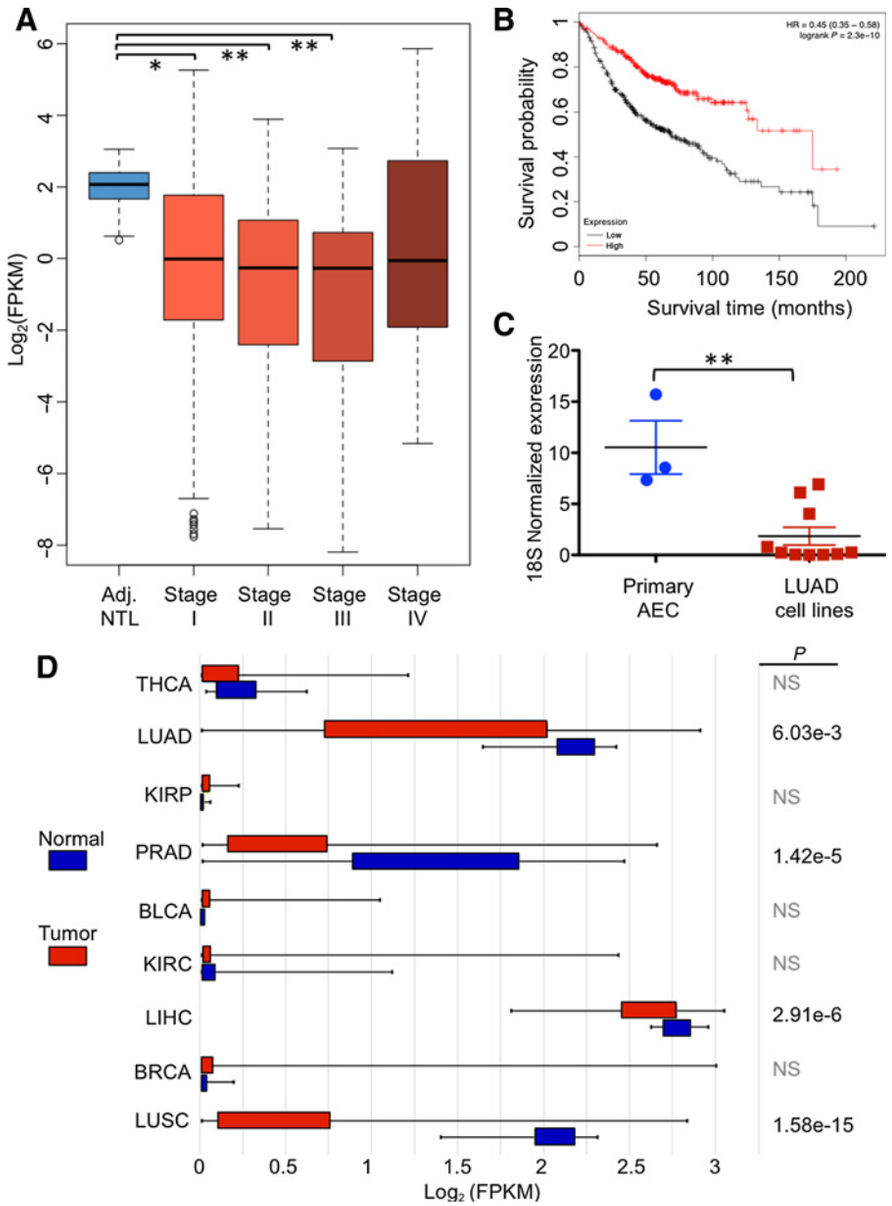

Figure 1.

Loss of *LINC00261* expression is correlated with decreased survival in lung adenocarcinoma. **A,** Stratification of *LINC00261* expression of 515 LUAD samples from TCGA (12) dataset by stage. Adj. NTL, adjacent nontumor lung. ANOVA tested all groups; difference is significant between normal and stages 1, 2, and 3. Stage 4 = ns (TANRIC; ref. 45). **B,** Overall survival of patients stratified by expression level of *LINC00261* derived from KMplot (46). Red, high *LINC00261* expression; black, low *LINC00261* expression. **C,** qRT-PCR of *LINC00261* expression in LUAD cell lines and the primary AECs. **D,** Stratification of *LINC00261* expression in multiple TCGA (12) datasets (lncRNAtor; ref. 34). See TCGA website for acronym definitions (https://cancergenome.nih.gov). *, $P \leq 0.05$; **, $P \leq 0.01$; NS, nonsignificant.

with this, we began to observe an increase in cells with higher order DNA content as evidenced by the increase in macronucleated cells (Supplementary Fig. S4B). These cells accounted for approximately 10%–15% of the population at any given time, similar to our FACS findings.

Bioinformatic profiling and pathways analysis of *LINC00261* targets

To determine the major pathways affected by *LINC00261* function, we performed RNA sequencing (RNA-seq) on the H522-CMV-NEO and H522-CMV-*LINC00261*–stable cell lines. RNA-seq analysis indicated that 108 genes were differentially expressed upon ectopic *LINC00261* reintroduction (Fig. 4A and B; Supplementary Table S3). Ingenutiy Pathways Analysis (IPA) revealed that the major pathways altered were G_2–M DNA damage checkpoint signaling, GADD45, and RAN signaling (Fig. 4C, blue bars). We then analyzed publicly available datasets to determine which genes and related pathways were significantly correlated to *LINC00261* expression levels. To do so, we utilized the TANRIC database, which has calculated coexpression networks for differentially expressed lncRNAs in numerous cancers. A total of 342 genes were significantly correlated with the expression of *LINC00261* in LUAD from TCGA RNA-seq profiling ($P < 1.0E{-}15$, normals are excluded from this analysis). Performing enrichment analysis on those correlated genes indicated that G_2–M cell-cycle arrest and the DNA damage response (DDR) were the top correlated pathways (Fig. 4C, purple bars). Strikingly, *LINC00261* reintroduction caused an upregulation in mRNA levels of ATM kinase, TOP2A, DNA helicase, and other critical members of the DDR pathway (Fig. 4D). Many of the same genes had expression correlated to *LINC00261* levels in TCGA LUAD gene expression profiling (Supplementary Fig. S5A and S5B).

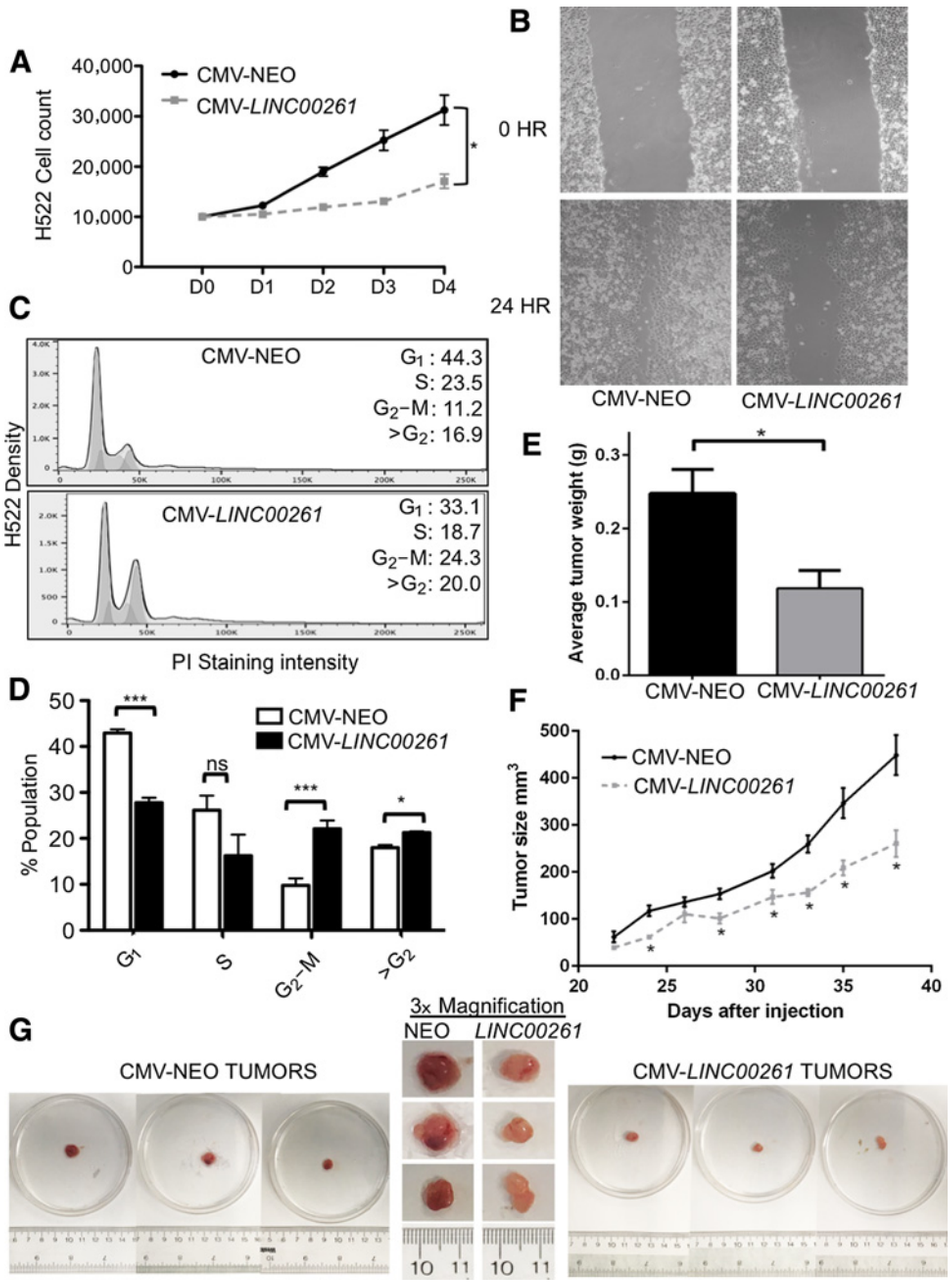

Figure 2.

Ectopic expression of *LINC00261* blocks proliferation and inhibits tumorigenesis through the induction of G_2–M cell-cycle arrest. **A,** Quantification of cell proliferation of H522-CMV-*LINC00261* and H522-CMV-NEO controls using Trypan blue staining. **B,** Scratch assay of H522-CMV-*LINC00261* cells compared with CMV-NEO vector control. Performed in three separate stable cell lines and technical quadruplicate ($N = 4$). Representative image shown. **C,** PI staining and FACS analysis of CMV-*LINC00261* and CMV-NEO controls. Population was analyzed using FlowJo v10.1. $N = 3$ ($\geq$10,000 cells per sample). Representative FACS analysis shown. **D,** Quantification of FACS analysis in **C**. **E,** Average weight of H522 xenograft tumors after excision. H522-CMV-NEO, 8 tumors; H522-CMV-*LINC00261*, 5 tumors. **F,** Size of xenograft tumors as measured over time. Significance was determined by a paired *t* test between test conditions at each time point as shown. *, $P < 0.05$. **G,** Images of tumors of H522 CMV-NEO and H522 CMV-*LINC00261* origin. Left, original images of tumors from CMV-NEO controls; right, tumors from CMV-*LINC00261*. The middle panel consists of $\times 3$ magnifications alongside ruler for size comparison. ***, $P \leq 0.001$; ns, nonsignificant.

The DNA damage pathway regulation is typically measured by the activation of protein phosphorylation. To determine whether there was altered phosphorylation of key DDR members, we performed phospho-specific antibody staining on lysates from H522-CMV-*LINC00261* alongside H522-CMV-NEO controls (Fig. 4E). This demonstrated that the reintroduction of *LINC00261* was able to increase the amount of detectable ATM phosphorylation, as well as phosphorylation of CHK2, a

downstream target of ATM. *LINC00261* reintroduction also increased the phosphorylation of BRCA2, as well as increased total levels of ATR and BRCA1 protein (Supplementary Fig. S5C). The increased activation of ATM in the presence of *LINC00261* was striking, as ATM is the sensor of DNA damage within the cell. To further assess whether *LINC00261* was acting upstream or downstream of ATM kinase, we treated both CMV-NEO and CMV-*LINC00261* cells with Ku-55933, a specific ATM inhibitor (36). Ku-55933 was able to block ATM phosphorylation as well as subsequent downstream phosphorylation events, indicating that *LINC00261* acts upstream of ATM activation to facilitate DNA damage response activation (Fig. 4E). Therefore, *LINC00261* may affect the ability of ATM to sense DNA damage and direct coordinated repair of the damaged loci.

Regulation of *LINC00261* by the pioneering transcription factor FOXA2

In searching for a mechanism by which *LINC00261* expression is regulated in cancer, we discovered that *LINC00261* is in a close genomic proximity to the pioneering transcription factor FOXA2. This transcription factor has critical regulatory functions in prostate, lung, liver, and overall endoderm development. FOXA2 is essential for normal differentiation of the alveolar epithelium, as FOXA2 ablation results in disrupted alveolarization (37). To determine whether FOXA2 plays a role in regulating *LINC00261* expression, we performed a correlation analysis using coexpression from the TANRIC database. *FOXA2* and *LINC00261* expression were highly correlated in LUAD ($R = 0.91$; $P = 3.5E{-}136$; Fig. 5A). In addition, expression of *LINC00261* was positively correlated to FOXA2 in several other epithelial cancers of endodermal origin, including hepatocellular carcinoma ($R = 0.66$; $P = 03.3E{-}5$), renal clear cell carcinoma ($R = 0.56$; $P = 3.3E{-}38$), prostate adenocarcinoma ($R = 0.702$; $P = 4.1E{-}22$), and lung squamous cell carcinoma ($R = 0.87$; $P = 4.8E{-}71$). Essentially all cancer types where *LINC00261* was found to be significantly downregulated in tumor versus normal comparisons were also highly correlated in expression to *FOXA2*. We then asked whether this effect was due to the regulation of *LINC00261* expression by FOXA2. To do this, we introduced ectopic CMV-FOXA2 into H522 cells, which lack endogenous *LINC00261* and FOXA2 expression. Ectopic reintroduction of FOXA2 stimulated the expression of endogenous *LINC00261 in trans* (Fig. 5B). However, when CMV-*LINC00261* was introduced into H522 cells, we did not find a concomitant increase in *FOXA2* expression (Fig. 5C), suggesting unidirectional regulation. To determine whether endogenous *LINC00261* could affect FOXA2 levels as reported previously (38), we utilized A549 cells, which have endogenous expression of *FOXA2* and *LINC00261*. shRNA-mediated ablation of *FOXA2* decreased endogenous expression of *LINC00261* (Fig. 5D). However, knockdown of *LINC00261* did not affect *FOXA2* levels (Fig. 5E).

FOXA2 is known to act as a pioneering transcription factor. We therefore utilized ENCODE FOXA2 ChIP-seq data in A549 cells to identify candidate FOXA2 transcription factor–binding sites that may affect *LINC00261* expression. We identified a FOXA2-binding site directly upstream of the *LINC00261* transcription start site and cloned this region into the pgl3 promoter luciferase reporter construct (Fig. 5F). Reporter cells containing the *LINC00261* promoter construct and minimal promoter vector controls were transfected alongside CMV-FOXA2 and CMV-NEO plasmid controls. We observed a significant increase in the overall promoter activity when comparing pgl3 empty vector to the vector containing the *LINC00261* promoter, indicating the promoter fragment was functional (Fig. 5G; $P = 0.0361$). In addition, CMV-FOXA2 transfection was able to stimulate *LINC00261* promoter activity significantly more than the empty vector control ($P = 0.0210$; Fig. 5G). The level of induction seen for the *LINC00261* promoter far exceeded the small increase observed for the reporter vector.

Epigenomic regulation of the *FOXA2-LINC00261* locus

Because loss of *FOXA2* and *LINC00261* expression were correlated in LUAD, and they occupy the same genomic locus, we sought to identify whether a common epigenetic mechanism of regulation was disrupted in cancer that could explain their mutual downregulation. We performed WGBS on purified AECs (27) and compared this to the WGBS profile of LUAD cell lines obtained from the Japanese database DBTSS. We observed that the *FOXA2-LINC00261* locus contains a 25 kB unmethylated domain in normal AECs and this region shows extensive hypermethylation in the majority of tested LUAD cell lines (Fig. 6A).

While the WGBS results suggested that DNA methylation may play a role in regulation of the *FOXA2-LINC00261* locus in LUAD, this experiment was performed on purified cells and cell lines. To determine whether a similar correlation in DNA methylation was observed in the primary tumors, we extracted the CpG methylation state and RNA expression levels from all LUAD TCGA tumors that had both data types available. Many of the CpG methylation sites surrounding the *LINC00261* (Supplementary Fig. S6A) promoter region showed hypermethylation in LUAD; the most statistically significant of those is shown in Fig. 6B. A significant negative correlation was observed between specific CpG methylation near the *FOXA2* (Fig. 6C) and *LINC00261* (Fig. 6D) promoters and their respective gene expression levels. Further examination of the DNMT family of enzymes implicates DNMT1 in the aberrant hypermethylation observed (Supplementary Fig. S6B).

Having established that hypermethylation was present at the FOXA2-*LINC00261* locus, we sought to understand the functional consequences on FOXA2 and *LINC00261* expression in LUAD. To test this, we extracted previously published reduced representation bisulfite sequencing information on A549 LUAD cancer cells treated for 13 days using multiple doses of 5-aza-cytidine (5-aza-CdR; ref. 39). This drug incorporates into DNA during replication and binds irreversibly to one of the major DNA methylation transferases, DNMT1, effectively inducing global demethylation. We observed decreased methylation of the CpG island proximal to the *LINC00261* transcription start site in the presence of 5-aza-CdR (Fig. 6E). This effect was observed at both tested doses compared with the vehicle controls. To determine whether the CpG island methylation status within the *FOXA2-LINC00261* locus could affect the transcriptional rate of *LINC00261* and hypermethylation of *FOXA2* promoter (Supplementary Fig. S7A), we subjected both *LINC00261* and *FOXA2* promoter constructs inserted into CpGLess vector to *in vitro* SssI-mediated methylation. Vector backbone with and without SssI methylation were used as normalization controls. Methylated and unmethylated constructs were then transfected into A549 cells, and a significant decrease in *LINC00261* promoter activity was observed (Fig. 6F). Hypermethylation also reduced the activity of the

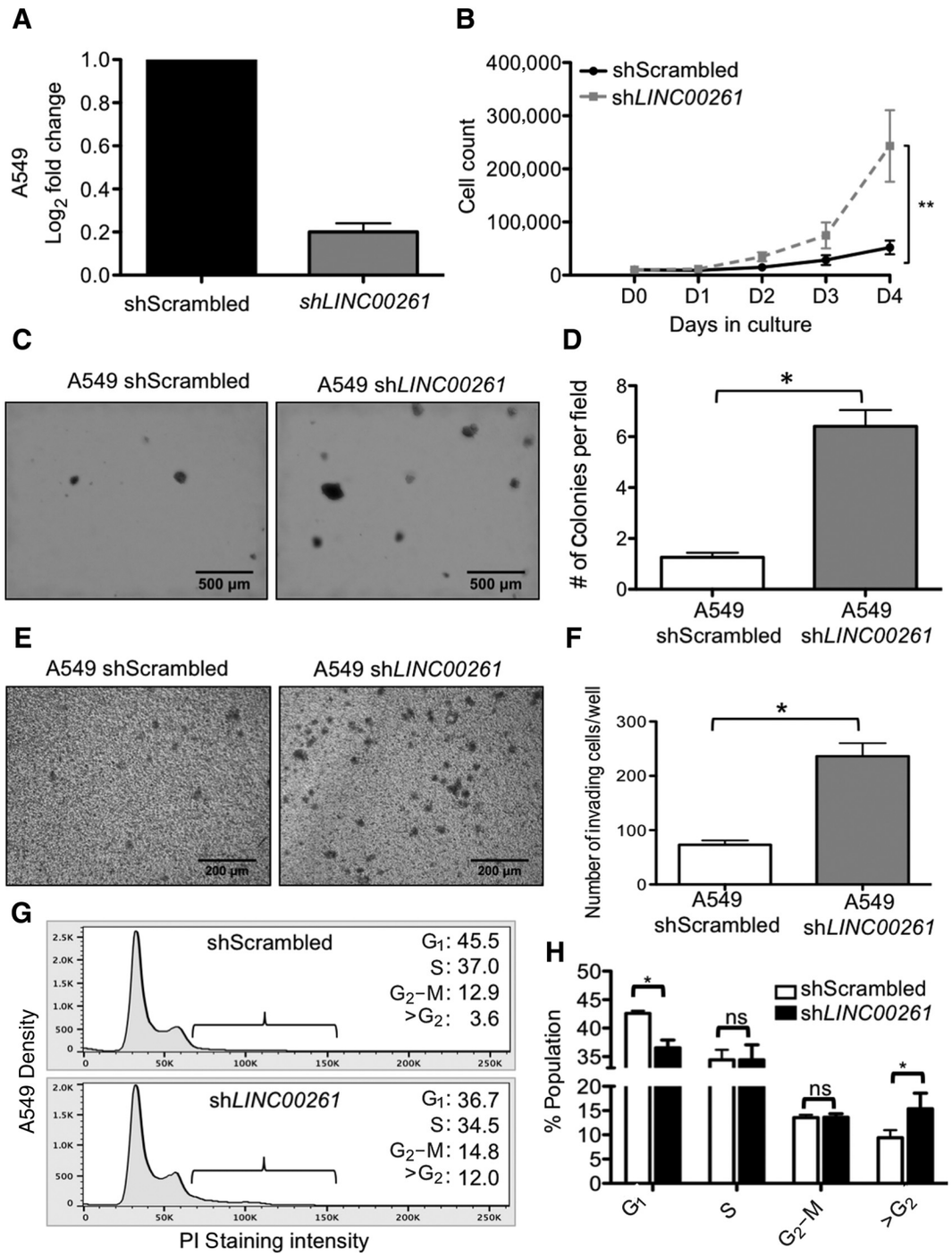

Figure 3.

Knockdown of *LINC00261* results in increased proliferation and migration in lung cell lines. **A,** Generation of stable A549 LUAD cell lines with short hairpin knockdown of *LINC00261*. Stable cell lines ($n = 3$) were generated and verified by qRT-PCR. **B,** Cell proliferation was counted using Trypan blue staining. Statistical analysis was performed on doubling times between stable cell lines shown ($N = 4$). **C,** Representative field (magnification, ×40) showing colony formation assay of A549-shScrambled and A549-sh*LINC00261* cells after 3 weeks of growth in 0.3% agar. **D,** Quantification of colony formation assay from counting colonies from three random fields in three biological replicates. Colony defined as area >10,000 μm^2. Significance calculated using a paired *t* test. **E,** Representative field (magnification, ×100) for cell invasion assay of A549-shScrambled and A549-sh*LINC00261* cells. **F,** Quantification of invasion assay from counting colonies from five random fields in three biological replicates. Statistical differences calculated using paired *t* test. **G,** Flow cytometric analysis of DNA content of LUAD cells using propidium iodide. Population was analyzed using FlowJo v10.1. $N = 3$ (≥10,000 cells per sample). Representative FACS analysis shown. **H,** Quantification of the flow analysis in **E**. Three biological replicates representing isolated stable clones were quantified in the technical triplicates. *, $P \leq 0.05$; **, $P \leq 0.01$; ns, nonsignificant.

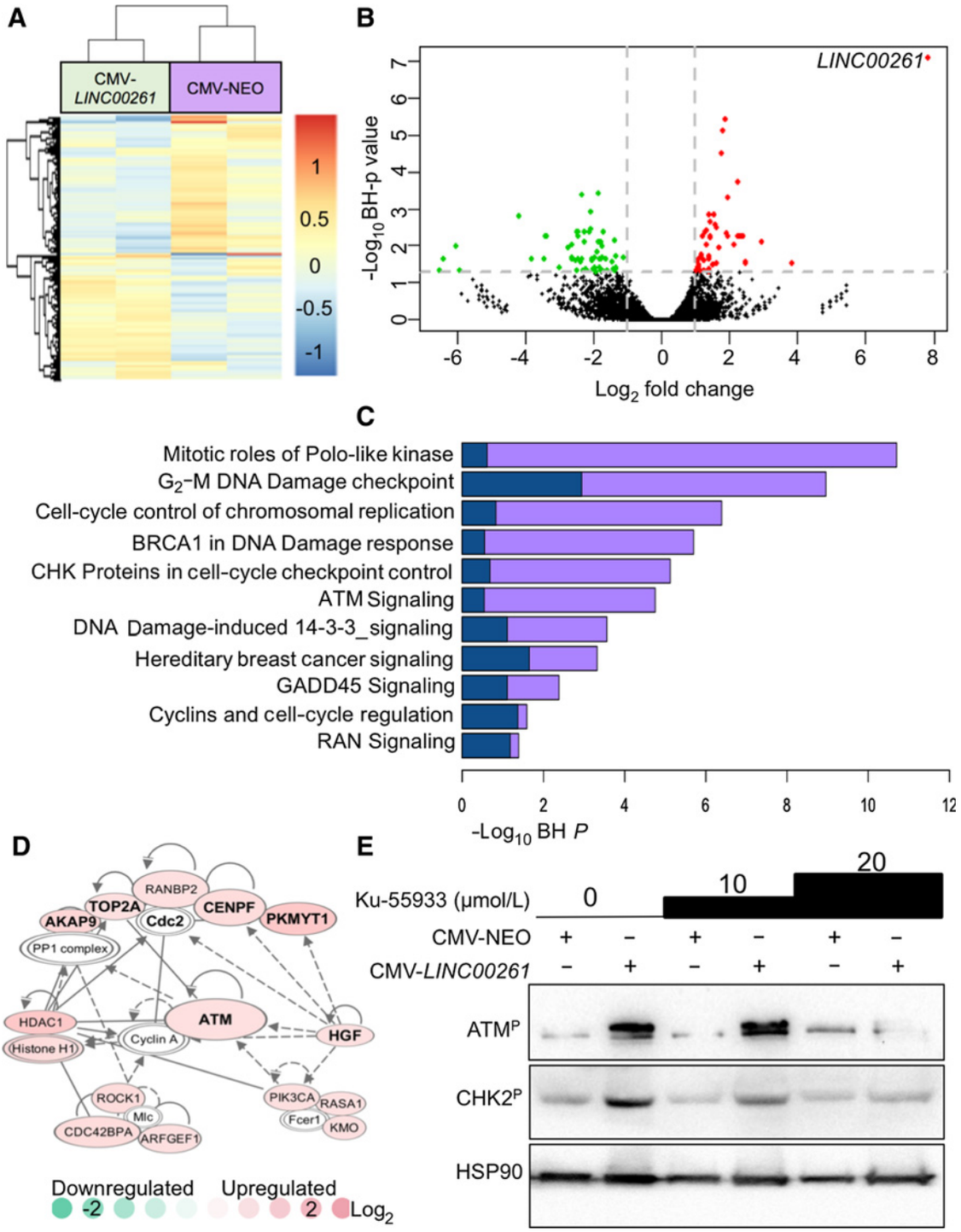

Figure 4.

RNA-seq analysis of H522 CMV-NEO and CMV-*LINC00261* stable cell lines reveals a role for *LINC00261* in the DNA damage pathway response. **A,** Unsupervised hierarchical clustering using ward method for reads per kilobase million (RPKM) of H522 CMV-NEO and CMV-*LINC00261* stable cell lines. Top 5% most variant genes shown. **B,** Volcano plot of the differential gene expression profiling. Red, upregulated in H522 CMV-*LINC00261*; green, downregulated in H522 CMV-*LINC00261*, as compared with H522 CMV-NEO control. **C,** IPA pathway enrichment of differentially expressed genes. Purple, correlated and anticorrelated genes with *LINC00261* expression in TCGA LUAD, as computed by TANRIC (45). Dark blue, differentially expressed genes between H522 CMV-NEO and CMV-*LINC00261*. Pathways are BH-corrected. **D,** IPA network analysis of significantly differentially expressed genes in the DNA damage response pathway with altered expression in the H522 CMV-*LINC00261* RNA-seq analysis. **E,** Western blotting of H522 CMV-NEO and H522 CMV-*LINC00261* upon exposure to multiple doses of ATM inhibitor Ku-55933.

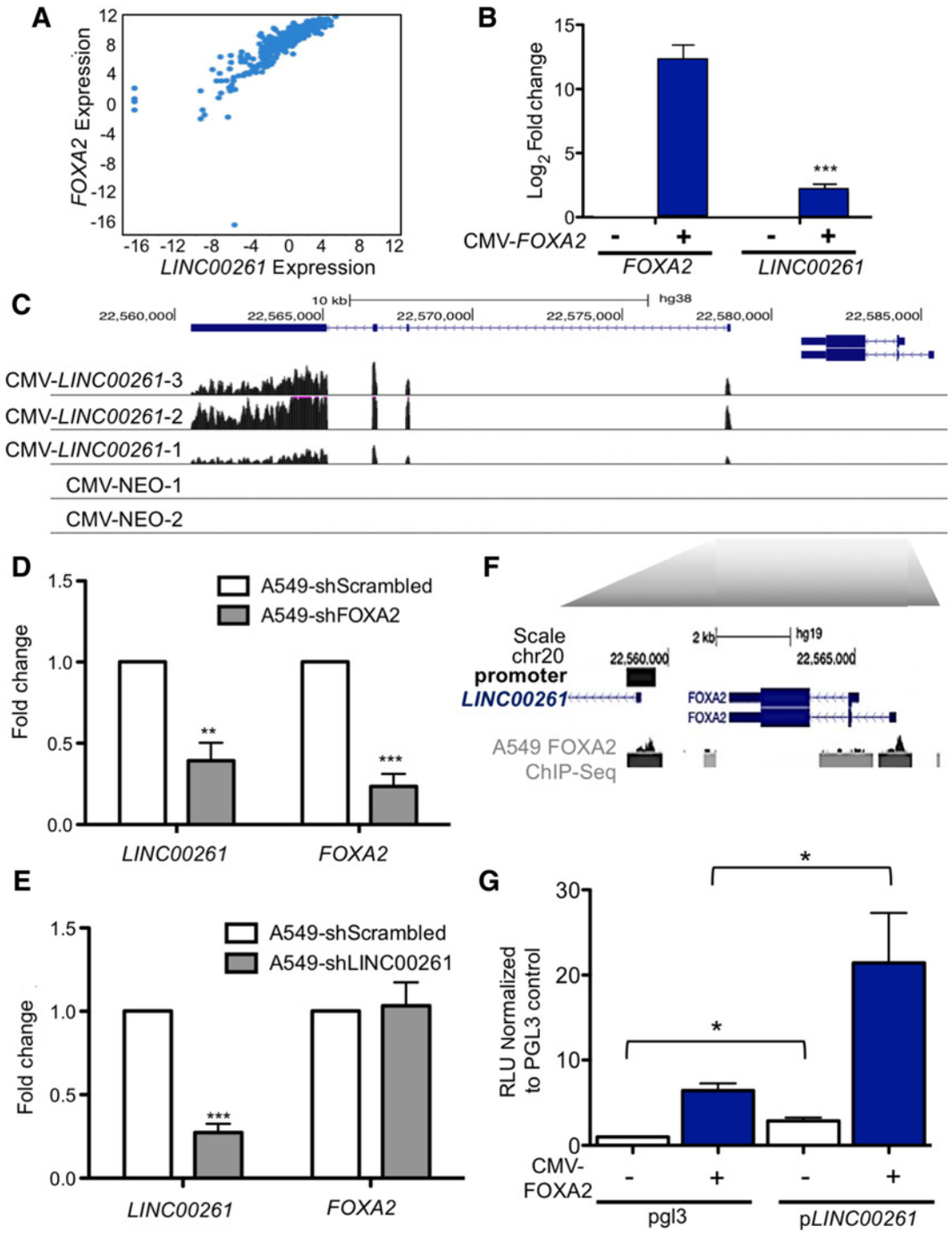

Figure 5.

FOXA2 regulates expression of *LINC00261* in LUAD. **A,** Correlation between FOXA2 and *LINC00261* expression from the TCGA LUAD dataset as computed by TANRIC (45). $R^2 = 0.91$. **B,** qRT-PCR of FOXA2 and *LINC00261* expression in H522 cells transiently transfected with CMV-FOXA2 or CMV-NEO control. *Y*-axis is (−) $\log_2$-fold change in expression between CMV-FOXA2 and CMV-NEO control. **C,** IGV image of BigWig tracks from H522-NEO and H522-CMV-*LINC00261* RNA-seq data. All tracks are scaled 0–100 for read depth. Each row is an independent stable cell line. **D,** qRT-PCR of FOXA2 and *LINC00261* expression in A549-sh*LINC00261* and A549-shScrambled controls. **E,** qRT-PCR of *FOXA2* and *LINC00261* expression in transiently transfected A549-shFOXA2 and A549-shScrambled controls. **F,** IGV image of cloned *LINC00261* promoter relative to the *LINC00261* transcription start site (promoter fragment is black). Gray, identified peaks from FOXA2 ChIP-seq in A549 cells generated by ENCODE. **G,** Luciferase assay in A549 cells of *LINC00261* promoter, activity in the presence or absence of transiently transfected CMV-FOXA2. Luciferase values are normalized to total protein content and corrected for background pgl3 luciferase activity. RLU, relative light units. A paired *t* test was used to determine the significance from four independent experiments, each with technical triplicates of plasmids derived from independent minipreps. *, $P \leq 0.05$; **, $P \leq 0.01$; ***, $P \leq 0.001$.

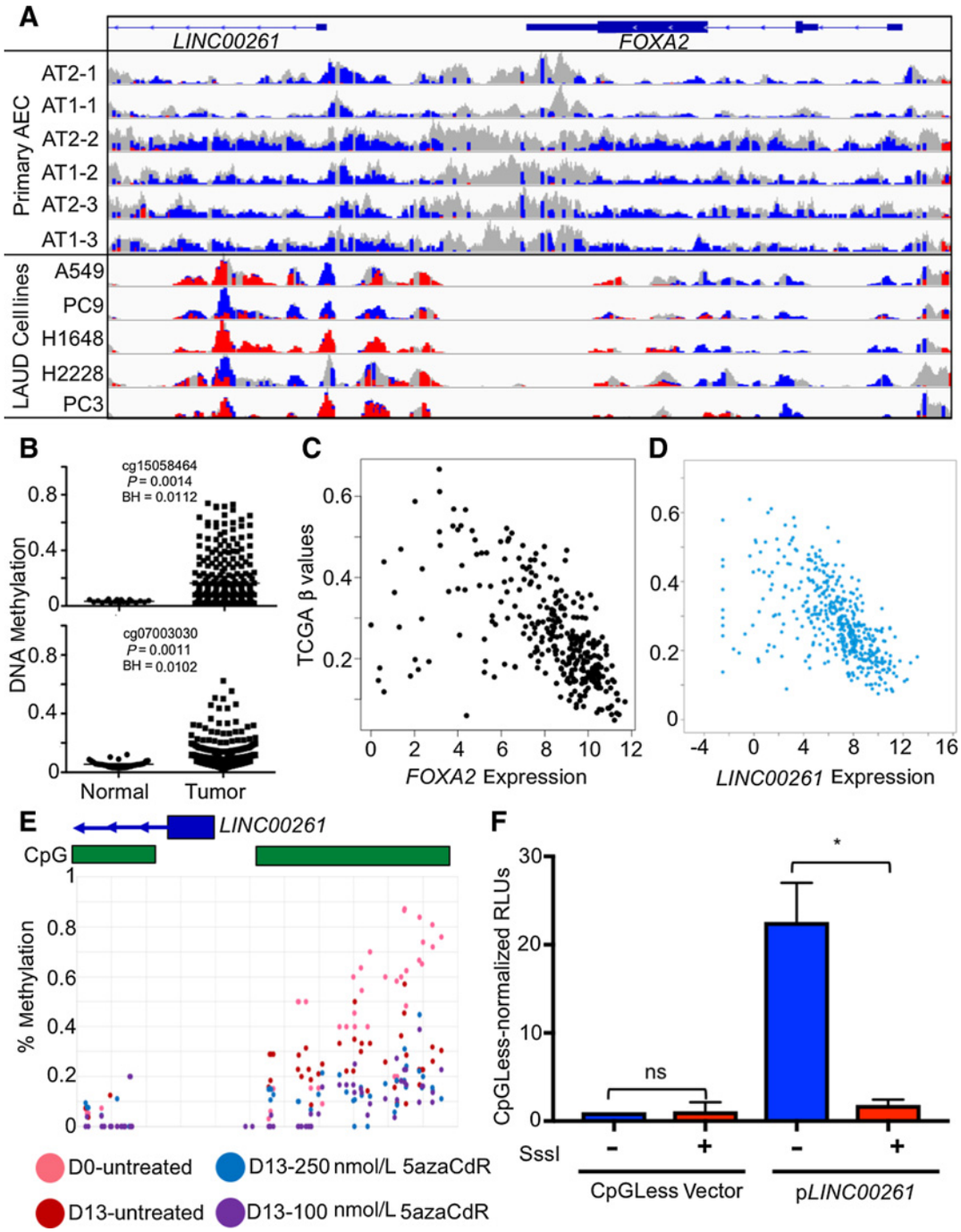

Figure 6.

The DNA hypermethylation deactivates expression at the *FOXA2/LINC00261* locus in LUAD. **A,** IGV track showing WGBS of the primary alveolar epithelial cells from three donor lungs and reduced representation bisulfite sequencing from DBTSS-generated LUAD cell lines. Red, methylated; blue, unmethylated; gray, non CpG sequence. **B,** Methylation of cg15058464 (*LINC00261* promoter, hg19 chr20:22,559,803, −523 from TSS) and cg07003030 (*FOXA2* promoter, hg19 chr20:22,565,995, −894 from TSS) in TCGA LUAD 450K array profiling (12) compared with adjacent tumor normal controls. **C,** Correlation between *FOXA2* and Infinium 450K, probe methylation in TCGA LUAD data for FOXA2 promoter ($R^2 = -0.56$). **D,** Correlation between *LINC00261* expression and Infinium 450K, probe methylation in TCGA LUAD for the *LINC00261* promoter (derived from cBioPortal, $R^2 = -0.41$). **E,** Methylation levels derived from reduced representation bisulfite sequencing of A549 cells treated with 5-azaCdR. Image shows percent methylation of multiple treatment conditions across the *LINC00261* promoter region. Green, CpG islands. **F,** Luciferase assay for the activity of *LINC00261* promoter in the presence or absence of *in vitro* SssI methylation. Data are normalized to CpGLess empty vector values from appropriate treatment group. A paired *t* test was performed on $N = 3$ biological replicates, each performed in technical triplicate. *, $P \leq 0.05$; ns, nonsignificant.

FOXA2 promoter; however, these results did not meet the threshold for statistical significance (Supplementary Fig. S7B). These results suggest that the hypermethylation of the *FOXA2-LINC00261* locus decreases the expression of both genes, resulting in a loss of downstream function.

Discussion

We have identified *LINC00261* as a noncoding RNA with tumor suppressor characteristics in LUAD and describe mechanistically how *LINC00261* could be responsible for the initial observations found in Liu and colleagues (40). *LINC00261* expression is lost in the vast majority of the primary LUAD tumors and cell lines. Reintroduction of *LINC00261* into LUAD cells was able to block proliferation, migration, and invasion capacity *in vitro*. Furthermore, we observed that *LINC00261* is an integral part of the DNA damage response in lung cells, without which the cells are unable to effectively initiate G_2–M cell-cycle arrest and the DNA damage repair signaling pathways critical for maintenance of healthy lung cells. In addition, we identified FOXA2 as a regulator of *LINC00261* expression, the regulation of which is disrupted in LUAD by hypermethylation of the entire *LINC00261-FOXA2* locus. Examination of RNA-seq expression levels suggest that increased expression of DMNT1 may be responsible for the observed hypermethylation; however, this would need to be further explored through detailed analysis of DNMT activity.

While our results point to the applicability of *LINC00261* as a tumor suppressor in other forms of endodermally derived epithelial lung cancers where FOXA2 is a critical transcription factor during development, we have not directly tested the effect of *LINC00261* on carcinogenesis in other cancer types. Even when restricted to LUAD, there is controversy as to whether FOXA2 functions as a tumor suppressor, as conflicting data exist within the literature. Our results suggest that the tumor-suppressive properties of FOXA2 may be mediated by its downstream target, *LINC00261*.

Many cancers exhibit global hypomethylation and localized hypermethylation in the CpG islands of gene promoters. However, many of these changes are thought to be passive events with little consequence on the overall proliferative and metastatic potential of the tumor (41). The observed epigenetic effect is interesting in the context of conflicting reports regarding the role of FOXA2 in lung cancer development. Many studies implicate FOXA2 as a tumor suppressor, equating this transcription factor as a differentiation signal that antagonizes cancer to help maintain the normal state. However, the actual mechanism by which FOXA2 exerts a tumor suppressing role is unknown, and there are also a few studies that demonstrate a pro-oncogenic role for FOXA2 in other epithelial cancers (42). Studies have evaluated the binding site affinity for FOXA2 (vs. the homolog FOXA1) and seen enrichment in lipid metabolism genes, none of which were implicated in its effect on carcinogenesis (43). Demonstration of a functional role for CpG island methylation at this locus suggests a possible causal role for DNA methylation in tumorigenesis by deactivating *LINC00261*. Therefore, differential epigenetic silencing of *LINC00261* in LUAD in specific contexts may resolve the confusion in the literature. Whether or not epigenetic silencing of the *LINC00261-FOXA2* locus plays a role in other cancer types remains to be tested. Our results also suggest that epigenetic therapies such as 5-azacytidine may be a viable alternate strategy for the treatment of LUAD and other epithelial cancers, as this could reactivate *LINC00261* and restore proper DNA damage response in these tumors.

We have therefore identified a lncRNA, *LINC00261*, which behaves as a tumor suppressor by blocking cellular proliferation through activation of the DNA damage signaling pathway to arrest cellular division. In addition, ATM, topoisomerase 2A (TOP2A), and other members of the DNA damage repair machinery have altered expression in the presence of *LINC00261*. Specifically, *LINC00261* has been reported to alter the efficacy of cisplatin therapy in colon cancer (44). Our study provides a mechanistic basis for this observation. In identifying a critical regulatory component of the DNA damage response, we have uncovered a new aspect of this critical pathway in carcinogenesis, one that opens up the possibility for the development of novel chemotherapeutic agents targeting this lncRNA to treat this deadly disease.

Disclosure of Potential Conflicts of Interest

No potential conflicts of interest were disclosed.

Authors' Contributions

Conception and design: B. Zhou, C.N. Marconett
Development of methodology: S. Shahabi, V. Kumaran, B. Zhou, C.N. Marconett
Acquisition of data (provided animals, acquired and managed patients, provided facilities, etc.): S. Shahabi, V. Kumaran, J. Castillo, Z. Cong, A. Saizan, R. Goel, A. Bhat, Z. Borok, C.N. Marconett
Analysis and interpretation of data (e.g., statistical analysis, biostatistics, computational analysis): V. Kumaran, J. Castillo, Z. Cong, D.J. Mullen, A. Alvarado, M.R. Correa, A. Saizan, R. Goel, S.K. Lynch, C.N. Marconett
Writing, review, and/or revision of the manuscript: S. Shahabi, V. Kumaran, J. Castillo, Z. Cong, G. Nandagopal, M.R. Correa, R. Goel, B. Zhou, Z. Borok, C.N. Marconett
Administrative, technical, or material support (i.e., reporting or organizing data, constructing databases): R. Goel, S.K. Lynch, C.N. Marconett
Study supervision: B. Zhou, Z. Borok, C.N. Marconett

Acknowledgments

We thank Dr. Ite A. Offringa for providing oversight and motivation to the project as well as the laboratory of Dr. Omid Akbari for assistance with cell-cycle analysis. In addition, we thank Charlie Nicolet, PhD, and the USC Epigenome Center for the generation of all sequencing data as well as Suhn Rhie, PhD, for assistance in manipulating the publicly available DBTSS whole-genome bisulfite sequencing data for easy visualization. Funding for the project was provided by the USC Department of Surgery, Research Fund, the Howard and Andree Shore STOP Cancer research fund, Baxter Foundation, and the Wright Foundation. This work was supported by in part by the Norris Comprehensive Cancer Center core grant, award number P30CA014089, from the National Cancer Institute. B. Zhou received support from Hastings and Whittier Foundations, the Will Rogers Institute, and research grant HL114959 from the NIH (Bethesda, MD). Z. Borok received support from Hastings and Whittier Foundations, the Will Rogers Institute, and research grant R35 HL135747 from the NIH (Bethesda, MD). Z. Borok is Ralph Edgington Chair in Medicine and Hastings Professor of Medicine.

The costs of publication of this article were defrayed in part by the payment of page charges. This article must therefore be hereby marked *advertisement* in accordance with 18 U.S.C. Section 1734 solely to indicate this fact.

Received July 11, 2018; revised December 21, 2018; accepted February 15, 2019; published first February 22, 2019.

References

1. Ridge CA, McErlean AM, Ginsberg MS. Epidemiology of lung cancer. Semin Intervent Radiol 2013;30:93–8.
2. Humphrey LL, Deffebach M, Pappas M, Zakher B, Slatore CG. Screening for lung cancer with low-dose computed tomography. Ann Intern Med 2014; 160:212.
3. Siegel RL, Miller KD, Jemal A. Cancer statistics, 2015. CA Cancer J Clin 2015;65:5–29.
4. Chen Z, Fillmore CM, Hammerman PS, Kim CF, Wong KK. Non-small-cell lung cancers: a heterogeneous set of diseases. Nat Rev Cancer 2014;14: 535–46.
5. Aggarwal S. Targeted cancer therapies. Nat Rev Drug Discov 2010;9:427–8.
6. Vanneman M, Dranoff G. Combining immunotherapy and targeted therapies in cancer treatment. Nat Rev Cancer 2012;12:237–51.
7. Cheng L, Alexander RE, Maclennan GT, Cummings OW, Montironi R, Lopez-Beltran A, et al. Molecular pathology of lung cancer: key to personalized medicine. Mod Pathol 2012;25:347–69.
8. Siegelin MD, Borczuk AC. Epidermal growth factor receptor mutations in lung adenocarcinoma. Lab Invest 2014;94:129–37.
9. Hata A, Katakami N, Yoshioka H, Fujita S, Kunimasa K, Nanjo S, et al. Erlotinib after gefitinib failure in relapsed non-small cell lung cancer: clinical benefit with optimal patient selection. Lung Cancer 2011;74:268–73.
10. Kobayashi S, Boggon TJ, Dayaram T, Jänne PA, Kocher O, Meyerson M, et al. EGFR mutation and resistance of non-small-cell lung cancer to gefitinib. N Engl J Med 2005;352:786–92.
11. Pao W, Miller VA, Politi KA, Riely GJ, Somwar R, Zakowski MF, et al. Acquired resistance of lung adenocarcinomas to gefitinib or erlotinib is associated with a second mutation in the EGFR kinase domain. PLoS Med 2005;2:e73.
12. The Cancer Genome Atlas Research Network. Comprehensive molecular profiling of lung adenocarcinoma. Nature 2014;511:543–50.
13. Seo JS, Ju YS, Lee WC, Shin JY, Lee JK, Bleazard T, et al. The transcriptional landscape and mutational profile of lung adenocarcinoma. Genome Res 2012;22:2109–19.
14. Derrien T, Johnson R, Bussotti G, Tanzer A, Djebali S, Tilgner H, et al. The GENCODE v7 catalog of human long noncoding RNAs: analysis of their gene structure, evolution, and expression. Genome Res 2012;22:1775–89.
15. Vance KW, Ponting CP. Transcriptional regulatory functions of nuclear long noncoding RNAs. Trends Genet 2014;30:348–55.
16. Mercer TR, Mattick JS. Structure and function of long noncoding RNAs in epigenetic regulation. Nat Struct Mol Biol 2013;20:300–7.
17. Geisler S, Coller J. RNA in unexpected places: long non-coding RNA functions in diverse cellular contexts. Nat Rev Mol Cell Biol 2013;14:699–712.
18. The Cancer Genome Atlas Research Network. Comprehensive genomic characterization of squamous cell lung cancers. Nature 2012;489:519–25.
19. Brunner AL, Beck AH, Edris B, Sweeney RT, Zhu SX, Li R, et al. Transcriptional profiling of long non-coding RNAs and novel transcribed regions across a diverse panel of archived human cancers. Genome Biol 2012;13:R75.
20. Zhang C, Wang X, Li X, Zhao N, Wang Y, Han X, et al. The landscape of DNA methylation-mediated regulation of long non-coding RNAs in breast cancer. Oncotarget 2017;8:51134–50.
21. Diaz-Lagares A, Crujeiras AB, Lopez-Serra P, Soler M, Setien F, Goyal A, et al. Epigenetic inactivation of the p53-induced long noncoding RNA TP53 target 1 in human cancer. Proc Natl Acad Sci U S A 2016;113:E7535–E44.
22. Cheetham SW, Gruhl F, Mattick JS, Dinger ME. Long noncoding RNAs and the genetics of cancer. Br J Cancer 2013;108:2419–25.
23. Iyer MK, Niknafs YS, Malik R, Singhal U, Sahu A, Hosono Y, et al. The landscape of long noncoding RNAs in the human transcriptome. Nat Genet 2015;47:199–208.
24. Prensner JR, Chinnaiyan AM. The emergence of lncRNAs in cancer biology. Cancer Discov 2011;1:391–407.
25. Castillo J, Stueve TR, Marconett CN. Intersecting transcriptomic profiling technologies and long non-coding RNA function in lung adenocarcinoma: discovery, mechanisms, and therapeutic applications. Oncotarget 2017;8: 81538–57.
26. Ishikawa Y, Kozakai T, Morita H, Saida K, Oka S, Masuo Y. Rapid detection of mycoplasma contamination in cell cultures using SYBR Green-based real-time polymerase chain reaction. In Vitro Cell Dev Biol Anim 2006;42: 63–9.
27. Marconett CN, Zhou B, Rieger ME, Selamat SA, Dubourd M, Fang X, et al. Integrated transcriptomic and epigenomic analysis of primary human lung epithelial cell differentiation. PLoS Genet 2013;9:e1003513.
28. Stueve TR, Li WQ, Shi J, Marconett CN, Zhang T, Yang C, et al. Epigenome-wide analysis of DNA methylation in lung tissue shows concordance with blood studies and identifies tobacco smoke-inducible enhancers. Hum Mol Genet 2017;26:3014–27.
29. Justus CR, Leffler N, Ruiz-Echevarria M, Yang LV. In vitro cell migration and invasion assays. J Vis Exp 2014. doi: 10.3791/51046.
30. Gebäck T, Schulz MM, Koumoutsakos P, Detmar M. TScratch: a novel and simple software tool for automated analysis of monolayer wound healing assays. Biotechniques 2009;46:265–74.
31. Liang CC, Park AY, Guan JL. In vitro scratch assay: a convenient and inexpensive method for analysis of cell migration in vitro. Nat Protoc 2007; 2:329–33.
32. Tomayko MM, Reynolds CP. Determination of subcutaneous tumor size in athymic (nude) mice. Cancer Chemother Pharmacol 1989;24:148–54.
33. White NM, Cabanski CR, Silva-Fisher JM, Dang HX, Govindan R, Maher CA. Transcriptome sequencing reveals altered long intergenic non-coding RNAs in lung cancer. Genome Biol 2014;15:429.
34. Park C, Yu N, Choi I, Kim W, Lee S. lncRNAtor: a comprehensive resource for functional investigation of long non-coding RNAs. Bioinformatics 2014;30:2480–5.
35. Cao WJ, Wu HL, He BS, Zhang YS, Zhang ZY. Analysis of long non-coding RNA expression profiles in gastric cancer. World J Gastroenterol 2013;19: 3658–64.
36. Stiff T, Walker SA, Cerosaletti K, Goodarzi AA, Petermann E, Concannon P, et al. ATR-dependent phosphorylation and activation of ATM in response to UV treatment or replication fork stalling. EMBO J 2006;25:5775–82.
37. Wan H, Xu Y, Ikegami M, Stahlman MT, Kaestner KH, Ang SL, et al. Foxa2 is required for transition to air breathing at birth. Proc Natl Acad Sci U S A 2004;101:14449–54.
38. Jiang W, Liu Y, Liu R, Zhang K, Zhang Y. The lncRNA DEANR1 facilitates human endoderm differentiation by activating FOXA2 expression. Cell Rep 2015;11:137–48.
39. Hascher A, Haase AK, Hebestreit K, Rohde C, Klein HU, Rius M, et al. DNA methyltransferase inhibition reverses epigenetically embedded phenotypes in lung cancer preferentially affecting polycomb target genes. Clin Cancer Res 2014;20:814–26.
40. Liu Y, Xiao N, Xu SF. Decreased expression of long non-coding RNA LINC00261 is a prognostic marker for patients with non-small cell lung cancer: a preliminary study. Eur Rev Med Pharmacol Sci 2017;21:5691–5.
41. Gutierrez-Arcelus M, Lappalainen T, Montgomery SB, Buil A, Ongen H, Yurovsky A, et al. Passive and active DNA methylation and the interplay with genetic variation in gene regulation. Elife 2013;2:e00523.
42. Wang B, Liu G, Ding L, Zhao J, Lu Y. FOXA2 promotes the proliferation, migration and invasion, and epithelial mesenchymal transition in colon cancer. Exp Ther Med 2018;16:133–40.
43. Bochkis IM, Schug J, Ye DZ, Kurinna S, Stratton SA, Barton MC, et al. Genome-wide location analysis reveals distinct transcriptional circuitry by paralogous regulators Foxa1 and Foxa2. PLoS Genet 2012;8:e1002770.
44. Wang ZK, Yang L, Wu LL, Mao H, Zhou YH, Zhang PF, et al. Long non-coding RNA LINC00261 sensitizes human colon cancer cells to cisplatin therapy. Braz J Med Biol Res 2017;51:e6793.
45. Li J, Han L, Roebuck P, Diao L, Liu L, Yuan Y, et al. TANRIC: an interactive open platform to explore the function of lncRNAs in cancer. Cancer Res 2015;75:3728–37.
46. Győrffy B, Surowiak P, Budczies J, Lánczky A. Online survival analysis software to assess the prognostic value of biomarkers using transcriptomic data in non-small-cell lung cancer. PLoS One 2013;8:e82241.